Seasonal variations in source-sink balance of CO_2 in subtropical earthen aquaculture ponds: Implications for carbon emission management

Lele Tang[a,b], Linhai Zhang[b,c,d], Ping Yang[a,b,c,d*], Chuan Tong[b,c,d], Hong Yang[e], Lishan Tan[f], Yongxin Lin[a,b,c], Derrick Y.F. Lai[f], Kam W. Tang[g*]

[a]*Fujian Provincial Key Laboratory for Subtropical Resources and Environment, Fujian Normal University, Fuzhou 350117, P.R. China*

[b]*School of Geographical Sciences, Fujian Normal University, Fuzhou 350117, P.R. China*

[c]*Key Laboratory of Humid Subtropical Eco-geographical Process of Ministry of Education, Fujian Normal University, Fuzhou 350117, P.R. China*

[d]*Wetland Ecosystem Research Station of Minjiang Estuary, National Forestry and Grassland Administration, Fuzhou 350215, P.R. China*

[e]*Department of Geography and Environmental Science, University of Reading, Reading, UK*

[f]*Department of Geography and Resource Management, The Chinese University of Hong Kong, Hong Kong, China*

[g]*Department of Biosciences, Swansea University, Swansea SA2 8PP, U. K.*

***Correspondence to:**

Ping Yang (yangping528@sina.cn); Kam W. Tang (k.w.tang@swansea.ac.uk)

A B S T R A C T

Aquaculture ponds sever as focal points for carbon cycling and act as anthropogenic contributors to the emission of carbon dioxide (CO_2). To understand the seasonal CO_2 dynamics within the ponds, we measured the CO_2 concentrations in sediment porewater and the water column in aquaculture ponds in the Shanyutan Wetland in China. Subsequently, the sediment-to-water and water-to-air CO_2 fluxes were calculated based on the gas transfer coefficient model. Our results showed that that CO_2 flux ranged 0.01–4.58 mmol m^{-2} h^{-1} across the sediment-to-water interface and -0.08–0.45 mmol m^{-2} h^{-1} across the water-to-air interface throughout the farming period. Photosynthetic activity was the key driver of the temporal variations in water column CO_2 concentration and water-to-air CO_2 flux, while the change in porewater CO_2 concentration and sediment-to-water CO_2 flux were governed by sediment temperature which drive the microbial decomposition of organic matter. Based on a simple mass balance approach, the apparent CO_2 consumption (ACC) in the water column across all seasons ranged from 0.24 to 2.32 mmol m^{-2} h^{-1}, indicating that the pond water body had a high capacity to "consume" the excess CO_2. Our results highlight that the contrasting roles between the sediment compartment and water column compartment in CO_2 dynamics, and the possibility to manipulate ACC to reduce the aquaculture carbon footprint.

Keywords: Carbon dioxide; Aquaculture ponds; Carbon footprint; Photosynthesis; Climate impact

1. Introduction

Carbon dioxide (CO_2) is a major greenhouse gas, accounting for approximately 60% of the overall atmospheric radiative forcing (Le Quéré et al., 2018; IPCC, 2014). Since 1750, there has been a 150% increase in the global atmospheric CO_2 concentration, reaching 417.2 ppm in 2022 (Friedlingstein et al., 2022), with many aquatic systems (e.g. lakes, reservoirs, rivers) acting as important CO_2 sources to the atmosphere (Borges et al., 2015; Li et al., 2018; Raymond et al., 2013; Tangen et al., 2016; Tranvik et al., 2009).

Small and shallow ponds, being integral components of global aquatic ecosystems, are hotspots for carbon cycling (Holgerson, 2015; Hou et al., 2023) and CO_2 emission (Holgerson and Raymond, 2016; Jensen et al., 2023; Prėskienis et al., 2021; Zhang et al., 2023). Small-scale aquaculture ponds are extensively found across various locations (FAO, 2018; Kosten et al., 2020; Luo et al., 2022), covering about 5.4×10^5 km^2 of surface area by 2016 (FAO, 2016). CO_2 emission from aquaculture has gained much attention (MacLeod et al., 2020) thanks to the fast-growing aquaculture sector world-wide (Naylor et al., 2021). In developing countries, unfortunately, proper monitoring of small-scale aquaculture ponds is often lacking (Soares and Henry-Silva, 2019; Xu et al., 2023; Zhang et al., 2022). Generally, these aquaculture ponds receive substantial quantities of organic matter as feeds, autochthonous carbon input and animal wastes (Chen et al., 2015; Tong et al., 2020). Organic carbon deposited into the sediment could be remineralized into CO_2 (Yang et al., 2022a); processes such as diffusion and bioturbation at the sediment-water interface would then determine the CO_2 flux to the overlying water (Gruca-Rokosz and

63 Tomaszek, 2015; Xiong et al., 2017). Meanwhile, processes within the water column
64 would further modulate the gains and losses of CO_2 (Morales-Williams et al., 2017, 2021;
65 Yang et al., 2022b), which would then determine the magnitude and direction of CO_2 flux
66 across the water-air interface.

67 In China, small-scale earthen shrimp ponds are among the fastest growing aquaculture
68 systems (Duan et al., 2020; Ren et al., 2019), many of which were created by clearing
69 areas of coastal wetlands. The Shanyutan Wetland is one the largest wetlands in Fujian,
70 China. Large swaths of the Shanyutan Wetland were converted to shrimp ponds in the past
71 decades, but environmental monitoring of the aquaculture operation here has been lacking
72 (Tong et al., 2020; Yang et al., 2022b), but which will be critical to assess its carbon
73 footprint and climate impact. We have recently begun to investigate the greenhouse gas
74 dynamics in these aquaculture ponds, and observed that the water-to-air CO_2 flux varied
75 seasonally, and was negative during certain time of the year (i.e., CO_2 going from air into
76 water) (Tan et al., 2023). This suggests capacity for the aquaculture ponds to switch
77 between being a CO_2 source and a CO_2 sink. To fully understand this source-sink dynamics,
78 it is necessary to include sediment CO_2 flux data and study how it varies seasonally.

79 In this study, the concentration of CO_2 was measured in both the water column and
80 the sediment porewater, and the sediment-to-water and water-to-air CO_2 fluxes were
81 calculated. Using a simple mass balance approach, we examined the CO_2 source-sink
82 balance within the aquaculture ponds, how it was influenced by environmental factors and
83 varied between seasons. This research aimed to determine the seasonal variations in CO_2

fluxes across the sediment-water-air interfaces and its main driving factors.

2. Materials and methods

2.1. Study area

The Shanyutan Wetland (22°00′36″26°03′42″N, 119°34′12″–119°41′40″E, Figure 1) in the Fujian Province, China, served as the location for this study. Situated at the southern tip of the Min River Estuary, the region experieces a subtropical marine monsoon climate characterized by an average air temperature of 19.6 °C and 139 cm of precipitation per year (Yang et al., 2020a, 2023). The dominant vegetation in the area consists of native species such as *Cyperus malaccensis* and *Phragmites australis*, along with the invasive *Spartina alterniflora* (Tan et al., 2023; Tong et al., 2018). Extensive areas of the tidal saltmarshes were cleared and converted to aquaculture shrimp ponds over the past decades (Yang et al., 2020b). Shrimp farming typically take place from May to November, yielding a single crop per year.

2.2. Collection of sediment and water samples

Three shrimp (*Litopenaeus vannamei*) ponds were selected for the study (Figure 1). Each pond was ~1.5 m deep and had an area of 1.5–2.0 ha. Field sampling was carried out monthly from April 2019 to January 2020. Samples of sediment and water were collected from three different locations with each pond: one near the bank, one in the feeding zone, and one at the center of the pond (Tian et al., 2023). The upper 15 cm sediments were collected using a steel cylinder with a diameter of 5 cm then transferred into sterile plastic bags. For the water column samples, a 1.5-L organic glass hydrophore was utilized to

105 collect samples from the surface layer (approximately 10 cm below the surface), mid-
106 depth, and the bottom layer (around 5 cm above the sediment). The collected water
107 samples were immediately divided into two portions. One portion of the water sample was
108 transferred into a pre-weighed serum glass bottle (55 mL) without bubbles and preserved
109 with 0.5 mL $HgCl_2$ for the analyses of dissolved CO_2 concentrations (Zhang et al., 2021).
110 The other portion was transferred into a 150 mL polyethylene bottle for analyzing physico-
111 chemical characteristics and chlorophyll *a* (Chl-*a*) concentrations. Prior to analysis in the
112 laboratory, the samples were stored in the dark at 4 °C for 4–6 hours.

113 *2.3. Analyses of sediment and water samples*

114 Sediment water content (SWC), bulk density (BD) and sediment porosity (POR) were
115 measured in the laboratory using a subsample from each sediment sample. The
116 measurement was based on weight loss before and after drying the subsample (Yin et al.,
117 2019; Zhang et al., 2013). The freeze-dried subsample was subjected to homogenization
118 and grinding until it formed a fine powder. Afterward, some of the powder was mixed with
119 deionized water in a 1:2.5 ratio (v/v) for measuring pH (Orion 868 pH meter, USA) and
120 in 1:5 ratio for measuring salinity (Eutech Instruments-Salt6 salinity meter, USA).
121 Sediment total carbon (TC) was measured via an elemental analyzer (Elementar Vario
122 MAX CN, Germany).

123 Porewater in raw sediment samples was extracted by centrifugation (Cence® L550,
124 Bodmer et al., 2020; De Vittor et al., 2012; Matos et al., 2016). Acetate fiber membranes
125 (0.45 μm-Biotrans™ nylon membranes) were employed to filter approximately 20 mL of

porewater and 100 mL of water column sample. The filtrates were analysed for the concentrations of Cl^- and SO_4^{2-} using an ion chromatograph (Dionex 2100, USA), and PO_4^{3-}-P, NH_4^+-N and NO_3^--N using a flow injection analyzer (Skalar Analytical SAN^{++}, Netherlands). Concentrations of DOC in sediment porewater were analyzed with a TOC Analyzer (TOC-$_{VCPH/CPN}$, Shimadzu, Japan). Furthermore, Chl-*a* in water column samples was extracted in 90% ethanol solution for 24 h and measured on a UV–visible spectrophotometer (Shimadzu UV-2450, Japan) (Jeffrey and Humphrey, 1975; Kang et al., 2023; Xu et al., 2017). In each sampling campaign, ancillary data including water temperature (T_W), sediment temperature (T_S), and dissolved oxygen (DO) were measured with a portable temperature meter (IQ150, USA) and a multiparameter probe (550A YSI, USA). Air temperature (T_A) and wind speed (W_S) were collected from the automatic meteorological station at the Min River Estuary (MRE) weather station.

2.4. Measurement of CO_2 concentration in water column and sediment porewater

The measurement of CO_2 concentration in water column and sediment porewater was conducted using the headspace equilibrium technique and a gas chromatograph (Bellido et al., 2009; Li et al., 2023; Zhang et al., 2021). A 6 mL subsample of sediment (or water) was transferred into a serum glass bottle with 24 mL of CO_2-free water (Dutta et al., 2015; Yang et al., 2019a). After the bottle was sealed, nitrogen gas (N_2) with a purity exceeding 99.999 %) was injected to replace a 25-mL headspace. The sealed bottle was then placed in an oscillator (IS-RDD3, China) and shaken for 10 min to reach an equilibrium in CO_2 concentration. After settling for 30 minutes, 5 ml of the headspace was extracted and

147 introduced into a gas chromatograph (GC-2010, Shimadzu, Japan). The gas
148 chromatograph was equipped with a flame ionization detection (FID) for CO_2. The
149 dissolved CO_2 concentrations (μmol CO_2 L^{-1}) in sediment porewater and water column
150 were calculated according to Ding et al. (2010) and Wanninkhof (1992).

151 *2.5. Diffusive CO_2 fluxes across the sediment-water interface and water-air interface*

152 Calculation of diffusive CO_2 fluxes across the sediment-water interface ($F_{S\text{-}W}$, mmol
153 m^{-2} h^{-1}) followed the methods proposed by Tan (2014) and Gruca-Rokosz and Tomaszek
154 (2015):

155 $$F_{S-W} = D_S \times \Delta C/\Delta Z = (D_w \times \varphi^2) \times (C_S - C_W)/\Delta Z \quad \text{(Eq. 1)}$$

156 where D_S (cm^2 s^{-1}) and D_w (cm^2 s^{-1}) are the diffusion coefficients of CO_2 in sediment and
157 water, respectively; $\Delta C/\Delta Z$ is the depth gradient of dissolved CO_2 concentration (μmol L^{-1}
158 cm^{-1}); C_S and C_W are the dissolved CO_2 concentrations (μmol L^{-1}) in sediment porewater
159 and overlying water, respectively; φ is the sediment porosity. D_W was calculated as:

160 $$D_W = 3.7 \times 10^{-11}T^3 + 2.6 \times 10^{-9}T^2 + 3.1 \times 10^{-7}T + 9.2 \times 10^{-6} \quad \text{(Eq. 2)}$$

161 where T was the sediment temperature (°C). $F_{S\text{-}W}$ was expressed in mmol m^{-2} h^{-1} with the
162 proper unit conversion, and positive values represented CO_2 flux from sediment into the
163 water column.

164 Diffusive CO_2 fluxes across the water-air interface ($F_{W\text{-}A}$, mmol m^{-2} h^{-1}) was calcula
165 ted according to Musenze et al. (2014):

166 $$F_{W-A} = [2.07 + (0.215 \times U_{10}^{1.7})] \times (Sc/660)^{-n} \times (C_W - C_{eq}) \quad \text{(Eq. 3)}$$

167 where U_{10} was the frictionless wind speed (m s^{-1}) at a height of 10 m above the water

surface (Crusius and Wanninkhof, 2003); *Sc* was the Schmidt number for CO_2, which was dependent on *in situ* water temperature and salinity, and was calculated according to Wanninkhof (1992); *n* was the proportionality coefficient that ranges from 0.50 (wind speed > 3 m s^{-1}) to 0.66 (for wind speed ⩽3 m s^{-1}) (Cole and Caraco, 1998); C_W was the dissolved CO_2 concentration (μmol L^{-1}) in the surface water at a depth of 20 cm; C_{eq} was the dissolved CO_2 concentration (μmol L^{-1}) at equilibrium with the atmosphere under the prevailing in *situ* conditions. $F_{S\text{-}W}$ was expressed in mmol m^{-2} h^{-1} with positive values representing CO_2 flux from surface water to air.

2.6. Data analysis

Water-column CO_2 concentrations within the aquaculture ponds would be determined by the balance between addition (e.g., through internal respiration and diffusive input) and subtraction (e.g., through photosynthesis and emission). We examined how this balance changed through time in two ways: First, because the sediment was a stronger diffusive source of CO_2 than the atmosphere (based on flux data), in the absence of thermal stratification (based on water temperature data), we assumed the bottom-layer CO_2 concentration to be the end-member value and the lower CO_2 concentrations in shallower depths would indicate photosynthetic consumption of CO_2. We therefore fitted a linear regression function to the depth-specific CO_2 concentrations for each month, with the slope ($\Delta CO_2/\Delta z$) indicating the rate of change in CO_2 with depth. For the second approach, we reasoned that if the pond water-column CO_2 pool was in a steady-state, CO_2 flux from sediment into water column ($F_{S\text{-}W}$) should equal CO_2 flux from surface water to air ($F_{W\text{-}}$

189 $_A$). Therefore, we calculated the seasonal average of F_{S-W} and F_{W-A}; the difference between
190 the two values would then represent the apparent CO_2 consumption (ACC) within the
191 water column due to autotrophic CO_2 fixation and/or CO_2 accumulation. Note that we used
192 the seasonal average values for this calculation to eliminate any short-term temporal and
193 spatial mismatch between F_{S-W} and F_{W-A}, and to illustrate the influence of seasonal
194 environmental conditions.

195 Taking the average depth-specific values for each month, we used two-way ANOVA
196 to examine the differences in Chl-*a* and CO_2 concentrations between months and depths.
197 One-way ANOVA was employed to assess temporal change in diffusive CO_2 fluxes (F_{S-W}
198 and F_{W-A}). Pearson's correlation analysis was employed to analyze the correlation between
199 environmental parameters and dissolved CO_2 concentration (or diffusive CO_2 fluxes)
200 using the vegan package in R (v. 4.1.0). Partial least square structural equation modeling
201 (PLS-SEM) was employed in software R (v. 3.5.3) with the 'semPLS' package to evaluate
202 the direct or indirect relationships between environmental variables and dissolved CO_2
203 concentration (or diffusive CO_2 fluxes). Details about the PLS-SEM analysis can be found
204 in Tan et al. (2022, 2023). A significance level of $p < 0.05$ was applied in all statistical
205 tests.

206 ## 3. Results

207 ### *3.1. Temperature, PO_4^{3-} and porewater CO_2*

208 Across the study period, the T_A, T_W and T_S ranged from 15.8–33.4 ºC, 14.7–32.1 ºC
209 and 14.8–25.4 ºC (Figure S1), respectively. T_W was nearly identical between depths for

each month (Figure S2). Temperatures were noticeably higher in the summer months (June-August) and early autumn (September-October). Water-column PO_4^{3-} concentrations remained low at around 60 µg L^{-1} for most of the months, except in autumn and early winter when it reached up to 138.9 µg L^{-1} (Figure 2a). Sediment porewater CO_2 concentration was rather low in spring (~53.2 µmol L^{-1}), but it increased steadily to 436.2 µmol L^{-1} in September, before it decreased sharply to 21.9 µmol L^{-1} by January (Figure 2b). The detailed results of other physico-chemical properties of sediment and water samples can be found in Supporting Information (Figures S3 and S4).

3.2. Water-column chlorophyll-a and CO_2 concentrations

The average Chl-*a* and CO_2 concentrations in the water column varied significantly between months and between depths (Table 1). Chl-*a* concentrations were higher in the surface layers, and it decreased slightly from spring to summer, then increased noticeably in autumn before dropping in winter (Figure 3a). The seasonal average Chl-*a* concentration varied between 86.9 and 175.8 µg L^{-1} throughout the study.

CO_2 concentrations increased sharply in the summer months, reaching a average of 27.4 µmol L^{-1}; it remained high in early autumn before it decreased sharply into late autumn and winter (Figure 3b). The vertical concentration gradient was also steeper in the summer. By fitting linear regression functions to the depth-specific CO_2 concentrations, the seasonal average rate of change was 2.26, 4.21, 1.25 and 0.20 µmol L^{-1} m^{-1} for spring, summer, autumn and winter, respectively (Figure 3b; Table S1).

3.3. Diffusive CO_2 fluxes and apparent CO_2 consumption

231 CO_2 flux across the sediment-water interface ($F_{S\text{-}W}$) varied significantly with time (p
232 < 0.001) and was always positive (i.e., CO_2 going from sediment to water) (Figure 4a). $F_{S\text{-}W}$ was low in spring, between 0.25 and 0.39 mmol m^{-2} h^{-1}; it then increased steadily to
234 4.58 mmol m^{-2} h^{-1} in September, before it decreased to 0.01 mmol m^{-2} h^{-1} by January.

235 Diffusive CO_2 flux across the water-air interface ($F_{W\text{-}A}$) varied significant with time
236 (p < 0.001) and was overall much lower than $F_{S\text{-}W}$ (Figure 4b). The $F_{W\text{-}A}$ values were
237 highest in the summer and early autumn, and close to zero or slightly negative (i.e., CO_2
238 going from air to water) in late autumn and winter.

239 We defined apparent CO_2 consumption (ACC) in the water column as the difference
240 between seasonal $F_{S\text{-}W}$ and $F_{W\text{-}A}$. The calculated ACC average value was positive for all
241 four seasons, meaning a net sink of CO_2 in the pond water body (Figure 4c). ACC was
242 highest in autumn (2.32 ± 1.01 mmol m^{-2} h^{-1}), followed by summer (1.02 ± 0.69) and
243 winter (0.41 ± 0.42), and it was lowest in spring (0.24 ± 0.14) (p<0.01).

244 *3.4. Environmental drivers of CO_2 concentrations and fluxes*

245 Pearson's correlation analysis showed that the water-column dissolved CO_2
246 concentration and $F_{W\text{-}A}$ was positively correlated with T_W and NO_3^--N (p<0.01), but
247 negatively correlated with DO, pH, salinity, PO_4^{3-}, Cl^-, SO_4^{2-} and Chl-*a* (p<0.01) (Figure
248 5a). The sediment porewater dissolved CO_2 concentration was positively correlated with
249 T_S, NO_3^--N, NH_4^+-N and DOC (p<0.05 or <0.01), but negatively with salinity, Cl^- and
250 SO_4^{2-} (p<0.05 or <0.01) (Figure 5b). $F_{S\text{-}W}$ was positively correlated with T_S, SWC, POR,
251 NO_3^--N and DOC (p<0.01), but negatively with salinity (p<0.01), SO_4^{2-} (p<0.001), BD

(p<0.01) and Cl^- (p<0.05) (Figure 5b).

As indicated in Figure 6a of the partial least square structural equation model (PLS-SEM), PO_4^{3-} had a positive effect on dissolved CO_2 in water column by way of Chl-*a*. Changes in $F_{W\text{-}A}$ were influenced by T_W and further mediated through changes in Chl-*a* and DO (Figure 6a). T_S and DOC positively affected $F_{S\text{-}W}$, directly and indirectly via porewater dissolved CO_2 (Figure 6b). $F_{S\text{-}W}$ was also negatively affected by SO_4^{2-} indirectly via P_{CO2} (Figure 6b).

4. Discussion

During the shrimp farming period between May and November, farmers added animal feeds twice per day to the ponds. The amount of added feeds increase as shrimp grow. Unconsumed feeds and animal wastes might settle to the bottom and add to sediment porewater CO_2 through decomposition (Hou et al., 2023; Lin and Lin, 2022; Xiong et al., 2017; Yang et al., 2019a), as reflected by the positive correlations between P_{CO2} and DOC and TC (Figure 5b). The higher sediment temperature in August and September (Figure S1) would have accelerated decomposition and increased porewater CO_2 concentration during that time (Figure 2b, 5b); this would also introduce remineralized nutrients such as PO_4^{3-} to the water column (Yang et al., 2019b), which was noticeable after a slight delay (Figure 2a). The increasing PO_4^{3-} concentration may explain the higher autotroph biomass (as Chl-*a*) (Lapointe et al., 2015; Morales-Williams et al., 2021) in the autumn (Figure 3a), as confirmed by correlation analysis (Figure 5a).

Water column CO_2 concentrations were higher in the summer, likely reflecting the

273 results of increasing respiration stimulated by the higher water temperatures (Figure 5a
274 and Figure S1; Yang et al., 2019a). Overall, the CO_2 concentrations in water column were
275 lower, sometimes by an order of magnitude, than sediment porewater CO_2 concentrations;
276 as a result, CO_2 would diffuse from the sediment to the overlying water, as confirmed by
277 the positive $F_{S\text{-}W}$ values (Figure 4a). The lower CO_2 concentrations in the upper water
278 column could be attributed to a higher photosynthetic CO_2 consumption in the shallower
279 water (Liu et al., 2010), driven by the higher Chl-*a* (Figure 3a) and light availability (Ni
280 et al., 2021; Ni et al., 2022), as supported by the strong negative correlation between W_{CO2}
281 and Chl-*a* (Figure 5a). Although the water-column Chl-*a* was highest in the autumn
282 (Figure 3b), the rate of change in CO_2 was largest in the summer (4.21 μmol L^{-1} m^{-1}),
283 likely because the higher seasonal light intensity and temperature (Figure S1) increased
284 the overall photosynthetic drawdown of CO_2.

285 Based on the concentration data, we calculated the CO_2 diffusive fluxes across the
286 sediment-water and water-air interfaces. While *in situ* CO_2 production within the sediment
287 did not necessarily translate directly to CO_2 diffusive flux, the seasonal variation in $F_{S\text{-}W}$
288 in this study was consistent with the seasonal variation in sediment CO_2 production
289 measured by slurry incubation (Tan et al., 2023), with higher values in the summer and
290 early autumn. $F_{S\text{-}W}$ value was positive throughout the study (Figure 4a), meaning that the
291 sediment was a consistent source of CO_2 for the water column.

292 The magnitude and seasonal pattern of $F_{W\text{-}A}$ were comparable to those measured
293 empirically with a floating chamber (Tan et al., 2023), with highest values in the summer

294 (Figure 4b). $F_{W\text{-}A}$ values were considerably lower than $F_{S\text{-}W}$, and in later autumn $F_{W\text{-}A}$ was
295 close to or below zero, indicating that the surface water acted as a CO_2 sink, which is also
296 consistent with earlier direct measurements (Tan et al., 2023).

297 By considering the overall CO_2 fluxes in and out of the aquaculture ponds across the
298 sediment-water and water-air interfaces, we can deduce the apparent CO_2 consumption
299 (ACC) within the water column, which would represent a combination of biological and
300 chemical fixation of CO_2, as well as accumulation of dissolved CO_2 in the water column.
301 We considered this to be "apparent" consumption because it did not include conversion of
302 CO_2 to other carbon gases (e.g. CH_4) and volatiles (Costa and Leigh, 2014; Elizabeth
303 Holmes et al., 2015; Li et al., 2023). ACC increased from spring to summer by >4 fold
304 (Figure 3a); however, the water-column CO_2 concentration increased only by 1.7-fold
305 between spring (seasonal average 15.98 μmol L^{-1}) and summer (27.42 μmol L^{-1}) (Figure
306 3b). Therefore, we suggest that much of the ACC was due to photosynthetic uptake, as
307 supported by the high rate-of-change in CO_2 through depth (Figure 3b). ACC was highest
308 in autumn, which coincided with an increase in Chl-*a* (Figure 3a) but not dissolved CO_2
309 (Figure 3b) in the water column, suggesting that the excess CO_2 had been incorporated
310 into autotroph and heterotroph biomass. This was consistent with the observations by Yang
311 et al. (2022b), who showed that the majority of the 'new' carbon within the aquaculture
312 ponds was introduced through photosynthesis. Some of the ACC in autumn could be
313 attributed to biomass harvested from the ponds, especially toward the end of the farming
314 period, but this is usually a small fraction (ca. 9-11%) of the carbon loss from the system

315 (Yang et al., 2022b).

316 Because CO_2 concentrations and fluxes could be influenced to different degrees and
317 in different directions by a multitude of variables (Figure 5), we used PLS-SEM to tease
318 out the key environmental factors and their effects (positive or negative) on CO_2
319 concentrations and fluxes. PLS-SEM results showed that temperature (T_w and T_s) had a
320 strong positive effect on CO_2 flux ($F_{W\text{-}A}$ and $F_{S\text{-}W}$, respectively) directly, or indirectly by
321 influencing other parameters (Figure 7). Higher temperature would increase the system
322 respiration and the mineralization of DOC thereby increasing CO_2 concentrations and
323 fluxes (Huttunen et al., 2003; Gudasz et al., 2010; Xiao et al., 2020; Yang et al., 2019). In
324 the water column, Chl-*a* and DO were the two key factors with a strong negative effect on
325 $F_{W\text{-}A}$ (Figure 7a), showing the importance of photosynthetic uptake of CO_2 (which releases
326 oxygen as byproduct) in determining the water-column CO_2 dynamics (Almeida et al.,
327 2016; Jensen et al., 2023; Morales-Williams et al., 2021; Yan et al., 2020). On the other
328 hand, DOC had the second strongest positive effect on $F_{S\text{-}W}$ (Figure 7b), showing that
329 decomposition of organic detritus within the sediment was the primary process in
330 controlling sediment-to-water CO_2 flux (Gruca-Rokosz and Tomaszek, 2015; Kristensen
331 et al., 2008; Xiong et al., 2017; Yang et al., 2019).

332 ## 5. Implications and conclusions

333 The fast-expanding aquaculture sector worldwide has raised concern about its
334 environmental impacts through effluent pollutions (Naylor et al., 2021) and greenhouse
335 gas emissions (MacLeod et al., 2020; Zhang et al., 2022). Decomposition of organic

carbon in the aquaculture pond sediment could produce both CO_2 and CH_4 (Yang et al., 2022a). Although the production rate of CH_4 in the sediment is orders of magnitude lower than that of CO_2 (Yang et al., 2022a), CH_4 is less soluble and could by-pass water-column consumption via ebullition (Tong et al., 2020), making aquaculture ponds hotspots for CH_4 emission (Zhang et al., 2022). In contrast, CO_2 dynamics within the aquaculture ponds is influenced by a more intricate network of gains and losses. In this study, significant temporal variations in dissolved CO_2 concentrations and fluxes were observed in the coastal aquaculture ponds. In addition to temperature, photosynthetic activity was the key driver of change in water column CO_2 concentration and water-to-air CO_2 flux. Porewater CO_2 concentration and sediment-to-water CO_2 flux were strongly influenced by sediment temperature, which would drive the microbial decomposition of organic matter.

Using a relatively simple system mass balance approach, we showed that, despite the strong and persistent source of CO_2 in the sediment, the water column had a high capacity to "consume" the excess CO_2, leading to a much lower than expected CO_2 emission to air; in some cases even a net sink of atmospheric CO_2. Understanding the underlying process and the potential to manipulate or enhance such a capacity, along with carbon burial into the sediment (Boyd et al., 2010; Yang et al., 2022b), may allow farmers to better assess and lower their carbon footprints.

Acknowledgements

This research received joint support from the National Natural Science Foundation of China (41801070, 41671088) and the Natural Science Foundation of Fujian Province

(2020J01136; 2022R1002006) .

References

Almeida, R.M., Nóbrega, G.N., Junger, P.C., Andrade, A.S., de Moura, C.G.B., Tonetta, D., Oliveira Jr, E.S., Araújo, F., Rust, F., Piñeiro-Guerra, J.M., Mendonça Jr, J.R., Medeiros, L.R., Pinheiro, L., Miranda, M., Costa, M.R.A., Melo, M.L., Nobre, R.L.G., Benevides, T., Roland, F., de Klein, J., Barros, N.O., Mendonça, R., Becker, V., Huszar, V.L.M., Kosten, S., 2016. High primary production contrasts with intense carbon emission in a eutrophic tropical reservoir. Front. Microbiol. 7(717), 1–13. https://doi.org/10.3389/fmicb.2016.00717

Bellido, J.L., Tulonen, T., Kankaala, P., Ojala, A., 2009. CO_2 and CH_4 fluxes during spring and autumn mixing periods in a boreal lake (paajarvi, southern finland). J. Geophys. Res.- Atmos. 114, G04007. https://doi.org/10.1029/2009jg000923

Bodmer, P., Wilkinson, J., Lorke, A., 2020. Sediment properties drive spatial variability of potential methane production and oxidation in small streams. J. Geophys. Res.- Biogeo. 125(1), e2019JG005213. https://doi.org/10.1029/2019JG005213

Borges, A.V., Darchambeau, F., Teodoru, C.R., Marwick, T.R., Tamooh, F., Geeraert, N., Omengo, F.O., Guérin, F., Lambert, T., Morana, C., Okuku, E., Bouillon, S., 2015. Globally significant greenhouse gas emissions from African inland waters. Nat. Geosci. 8(8), 637–642. https://doi.org/10.1038/NGEO2486

Boyd, C.E., Wesley Wood, C., Chaney, P.L., Queiroz, J.F., 2010. Role of aquaculture pond sediments in sequestration of annual global carbon emissions. Environ. Pollut. 158, 2537–2540. https://doi.org/10.1016/j.envpol.2010.04.025

Chen, Y., Dong, S.L., Wang, Z.N., Wang, F., Gao, Q.F., Tian, X.L., Xiong, Y.H., 2015. Variations in CO_2 fluxes from grass carp *Ctenopharyngodon idella* aquaculture polyculture ponds. Aquacult. Environ. Interac. 8, 31–40. https://doi.org/10.3354/aei00149

Cole, J.J., Caraco, N.F., 1998. Atmospheric exchange of carbon dioxide in a low-wind oligotrophic lake measured by the addition of SF_6. Limnol. Oceanogr. 43, 647–656. https://doi.org/10.4319/lo.1998.43.4.0647

Costa, K.C., Leigh, J.A., 2014. Metabolic versatility in methanogens. Curr. Opin. Biotech.

29, 70–75. https://doi.org/10.1016/j.copbio.2014.02.012

Crusius, J., Wanninkhof, R., 2003. Gas transfer velocities measured at low wind speed over a lake. Limnol. Oceanogr. 48(3), 1010–1017.

De Vittor, C., Faganeli, J., Emili, A., Covelli, S., Predonzani, S., Acquavita, A., 2012. Benthic fluxes of oxygen, carbon and nutrients in the marano and grado lagoon (northern adriatic sea, Italy). Estuar. Coast. Shelf S. 113, 57–70. https://doi.org/10.1016/j.ecss.2012.03.031

Ding, W.X., Zhang, Y.H., Cai, Z.C., 2010. Impact of permanent inundation on methane emissions from a *Spartina alterniflora* coastal salt marsh. Atmos. Environ. 44, 3894–3900. https://doi.org/10.1016/j.atmosenv.2010.07.025

Duan, Y.Q., Li, X., Zhang, L.P., Chen, D., Liu, S.A., Ji, H.Y., 2020. Mapping national-scale aquaculture ponds based on the Google Earth Engine in the Chinese coastal zone. Aquaculture 520, 734666. https://doi.org/10.1016/j.aquaculture.2019.734666

Dutta, M.K., Mukherjee, R., Jana, T.K., Mukhopadhyay, S.K., 2015. Biogeochemical dynamics of exogenous methane in an estuary associated to a mangrove biosphere; the Sundarbans, NE coast of India. Mar. Chem. 170, 1–10. https://doi.org/10.1016/j.marchem.2014.12.006

Elizabeth Holmes, M., Chanton, J.P., Tfaily, M.M., Ogram, A., 2015. CO_2 and CH_4 isotope compositions and production pathways in a tropical peatland. Global Biogeochem. Cy. 29(1), 1–18. https://doi.org/10.1002/ 2014GB004951

FAO. 2018. The State of World Fisheries and Aquaculture. Food and Agricultural Organization of the United Nations, Rome, Italy.

FAO, 2016. The State of World Fisheries and Aquaculture 2016 Contributing to Food Security and Nutrition for all. (Rome).

Friedlingstein, P., O'Sullivan, M., Jones, M.W., Andrew, R.M., Gregor, L., et al., 2022 Global Carbon Budget 2022. Earth Syst. Sci. Data 14, 4811–4900, https://doi.org/10.5194/essd-14-4811-2022

Gruca-Rokosz, R., Tomaszek, J.A., 2015. Methane and carbon dioxide in the sediment of a eutrophic reservoir: production pathways and diffusion fluxes at the sediment–water interface. Water Air Soil Poll. 226, 16. https://doi.org/10.1007/s11270-014-2268-3

Gudasz, C., Bastviken, D., Steger, K., Premke, K., Sobek, S., Tranvik, L.J., 2010.

418 Temperature-controlled organic carbon mineralization in lake sediments. Nature 466,
419 478–482. https://doi.org/10.1038/nature09186
420 Holgerson, M.A., 2015. Drivers of carbon dioxide and methane supersaturation in small,
421 temporary ponds. Biogeochemistry 124(1–3), 305–318.
422 https://doi.org/10.1007/s10533-015-0099-y
423 Holgerson, M.A., Raymond, P.A., 2016. Large contribution to inland water CO_2 and CH_4
424 emissions from very small ponds. Nat. Geosci. 9(3), 222–226.
425 https://doi.org/10.1038/ngeo2654
426 Hou, Y.X., Liu, Y., Zhang, J.X., Yu, X., 2023. Temporal dynamics of lateral carbon export
427 from an onshore aquaculture farm. Sci. Total Environ. 859, 160258.
428 http://dx.doi.org/10.1016/j.scitotenv.2022.160258
429 Huttunen, J.T., Alm, J., Liikanen, A., Juutinen, S., Larmola, T., Hammar, T., Silvola, J.,
430 Martikainen, P.J., 2003. Fluxes of methane, carbon dioxide and nitrous oxide in boreal
431 lakes and potential anthropogenic effects on the aquatic greenhouse gas emissions.
432 Chemosphere 52, 609–621. https://doi.org/10.1016/s0045-6535(03)00243-1
433 IPCC, 2014. Climate Change 2014: Synthesis Report. Contribution of Working Groups I,
434 II and III to the Fifth Assessment Report of the Intergovernmental Panel on Climate
435 Change. IPCC, Geneva, Switzerland.
436 Jeffrey, S.W., Humphrey, G.F., 1975. New spectrophotometric equations for determining
437 chlorophylls *a*, *b*, c_1 and c_2 in higher plants, algae and natural phytoplankton.
438 Biochemie Und Physiologie Der Pflanzen, 167(2), 191–194.
439 https://doi.org/10.1016/0022-2860(75)85046-0
440 Jensen, S.A., Webb, J.R., Simpson, G.L., Baulch, H.M., Leavitt, P.R., Finlay, K., 2023.
441 Differential controls of greenhouse gas (CO_2, CH_4, and N_2O) concentrations in natural
442 and constructed agricultural waterbodies on the Northern Great Plains. J. Geophys.
443 Res.-Biogeo. 128, e2022JG007261. https://doi.org/10.1029/2022JG007261
444 Kang, L.J., Zhu, G.W., Zhu, M.Y., Xu, H., Zou, W., Xiao, M., Zhang, Y.L., Qin, B.Q.,
445 2023. Bloom-induced internal release controlling phosphorus dynamics in large
446 shallow eutrophic Lake Taihu, China. Environ. Res. 231(Part 3), 116251.
447 https://doi.org/10.1016/j.envres.2023.116251
448 Kosten, S., Almeida, R.M., Barbosa, I., Mendona, R., Barros, N., 2020. Better assessments

449 of greenhouse gas emissions from global fish ponds needed to adequately evaluate
450 aquaculture footprint. Sci. Total Environ. 748, 141247.
451 https://doi.org/10.1016/j.scitotenv.2020.141247
452 Kristensen, E., Bouillon, S., Dittmar, T., Marchand, C., 2008. Organic carbon dynamics in
453 mangrove ecosystems: a review. Aquat. Bot. 2, 201–219.
454 https://doi.org/10.1016/j.aquabot.2007.12.005
455 Lapointe, B.E., Herren, L.W., Debortoli, D.D., Vogel, M.A., 2015. Evidence of sewage-
456 driven eutrophication and harmful algal blooms in Florida's Indian River Lagoon.
457 Harmful Algae 43, 82–102. http://dx.doi.org/10.1016/j.hal.2015.01.004
458 Le Quéré, C., Andrew, R.M., Friedlingstein, P., Sitch, S., Hauck, J., Pongratz, J., Pickers,
459 P.A., et al., 2018. Global Carbon Budget 2018, Earth Syst. Sci. Data 10, 2141–2194.
460 https://doi.org/10.5194/essd-10-2141-2018
461 Li, B., Wang, H.W., Lai, A.X., Xue, J.Y., Wu, Q., Yu, C.Y., Xie, K., Mao, Z.D., Li, H.B.,
462 Xing, P., Wu, Q.L., 2023. Hydrogenotrophic pathway dominates methanogenesis
463 along the river-estuary continuum of the Yangtze River. Water Res. 240, 120096.
464 https://doi.org/10.1016/j.watres.2023.120096
465 Li, S.Y., Bush, R.T., Santos, I.R., Zhang, Q.F., Song, K.S., Mao, R., Wen, Z.D., Lu, X.X.,
466 2018. Large greenhouse gases emissions from China's lakes and reservoirs. Water Res.
467 147, 13–24. https://doi.org/10.1016/j.watres.2018.09.053
468 Li, Y.X., Deng, K.K., Lin, G.J., Chen, B., Fang, F., Guo, J.S., 2023. Effects of
469 physiologic activities of plankton on CO_2 flux in the Three Gorges Reservoir after
470 rainfall during algal blooms. Environ. Res. 216(Part 3), 114649.
471 https://doi.org/10.1016/j.envres.2022.114649
472 Lin, G.M., Lin, X.B., 2022. Bait input altered microbial community structure and
473 increased greenhouse gases production in coastal wetland sediment. Water Research,
474 218(3), 118520. https://doi.org/10.1016/j.watres.2022.118520
475 Liu, Z.H., Dreybrodt, W. Wang, H.J., 2010. A new direction in effective accounting for the
476 atmospheric CO_2 budget: Considering the combined action of carbonate dissolution,
477 the global water cycle and photosynthetic uptake of DIC by aquatic organisms. Earth-
478 Sci. Rev. 99, 162–172. https://doi.org/10.1016/j.earscirev.2010.03.001
479 Luo, J.H., Sun, Z., Lu, L.R., Xiong, Z.Y., Cui, L.P., Mao, Z.G., 2022. Rapid expansion of

coastal aquaculture ponds in Southeast Asia: patterns, drivers and impacts. J. Environ. Manag. 315, 115100. https://doi.org/10.1016/j.jenvman.2022.115100

MacLeod, M.J., Hasan, M.R., Robb, D.H., Mamun-Ur-Rashid, M., 2020. Quantifying greenhouse gas emissions from global aquaculture. Sci. Rep. 10(1), 11679. https://doi.org/10.1038/s41598-020-68231-8

Matos, C.R.L., Mendoza, U., Diaz, R., Moreira, M., Belem, A.L., Metzger, E., Albuquerque, A.L.S., Machado, W., 2016. Nutrient regeneration susceptibility under contrasting sedimentary conditions from the Rio de Janeiro coast, Brazil. Mar. Pollut. Bull. 108, 297–302. https://doi.org/10.1016/j.marpolbul.2016.04.046

Morales-Williams, A.M., Wanamaker, A.D., Downing, J.A., 2017. Cyanobacterial carbon concentrating mechanisms facilitate sustained CO_2 depletion in eutrophic lakes. Biogeosciences 14, 2865–75. https://doi.org/10.5194/bg-14-2865-2017.

Morales-Williams, A.M., Wanamaker Jr., A.D., Williams, C.J., Downing, J.A., 2021. Eutrophication drives extreme seasonal CO_2 flux in lake ecosystems. Ecosystems 24, 434–450. https://doi.org/10.1007/s10021-020-00527-2

Musenze, R.S., Grinham, A., Werner, U., Gale, D., Sturm, K., Udy, J., Yuan, Z.G., 2014. Assessing the spatial and temporal variability of diffusive methane and nitrous oxide emissions from subtropical freshwater reservoirs. Environ. Sci. Technol. 48, 14499–14507. https://doi.org/10.1021/es505324h

Naylor, R.L., Hardy, R.W., Buschmann, A.H., Bush, S.R., Cao, L., Klinger, D.H., Little, D.C., Lubchenco, J., Shumway, S.E., Troell, M., 2021. A 20-year retrospective review of global aquaculture. Nature 591, 551–563. https://doi.org/10.1038/s41586-021-03308-6

Ni, M.F., Li, S.Y., 2022. Dynamics and internal links of dissolved carbon in a karst river system: Implications for composition, origin and fate. Water Res. 226, 119289. https://doi.org/10.1016/j.watres.2022.119289

Ni, M.F., Ge, Q.S., Li, S.Y., Wang, Z.K., Wu, Y.J., 2021. Trophic state index linked to partial pressure of aquatic carbon dioxide in a typical karst plateau lake. Ecol. Indic. 120, 106912. https://doi.org/10.1016/j.ecolind.2020.106912

Prėskienis, V., Laurion, I., Bouchard, F., Douglas, P.M.J., Billett, M.F., Fortier, D., Xu, X.M., 2021. Seasonal patterns in greenhouse gas emissions from lakes and ponds in a

High Arctic polygonal landscape. Limnol. Oceanogr. 66, S117–S141. https://doi.org/10.1002/lno.11660

Raymond, P.A., Hartmann, J., Lauerwald, R., Sobek, S., McDonald, C., Hoover, M., Butman, D., Striegl, R., Mayorga, E., Humborg, C., Kortelainen, P., Durr, H., Meybeck, M., Ciais, P., Guth, P., 2013. Global carbon dioxide emissions from inland waters. Nature 503, 355–359. https://doi.org/10.1038/nature12760

Ren, C.Y., Wang, Z.M., Zhang, Y.Z., Zhang, B., Chen, L., Xia, Y.B., Xiao, X.M., Doughty, R.B., Liu, M.Y., Jia, M., Mao, D.H., Song, K.S., 2019. Rapid expansion of coastal aquaculture ponds in China from Landsat observations during 1984–2016. Int. J. Appl. Earth Obs. 82, 101902. https://doi.org/10.1016/j.jag.2019.101902

Soares, D.C.E., Henry-Silva, G.G., 2019. Emission and absorption of greenhouse gases generated from marine shrimp production (*Litopeneaus vannamei*) in high salinity. J. Clean. Prod. 218, 367–376. https://doi.org/10.1016/j.jclepro.2019.02.002

Tan, L.S., Ge, Z.M., Ji, Y.H., Lai, D.Y.F., Temmerman, S., Li, S.H., Li, X.Z., Tang, J.W., 2022. Land use and land cover changes in coastal and inland wetlands cause soil carbon and nitrogen loss. Global Ecol. Biogeogr. 31, 2541–2563. https://doi.org/10.1111/geb.13597

Tan, L.S., Zhang, L.H., Yang, P., Tong, C., Lai, D.Y.F., Yang, H., Hong, Y., Tian, Y.L., Tang, C., Ruan, M.J., Tang, K.W., 2023. Effects of conversion of coastal marshes to aquaculture ponds on sediment anaerobic CO_2 production and emission in a subtropical estuary of China. J. Environ. Manag. 338, 117813. https://doi.org/10.1016/j.jenvman.2023.117813

Tan, Y.J., 2014. The greenhouse gases emission and production mechanism from river sediment in Shanghai. East China Normal University, Shanghai (Thesis, in Chinese).

Tian, Y.L, Yang, P., Yang, H., Wang, H.M., Zhang, L,H., Tong, C., Lai, D.Y.F., Lin, Y.X., Tan, L.S., Hong, Y., Tang, C., Tang, K.W., 2023. Diffusive nitrous oxide (N_2O) fluxes across the sediment-water-atmosphere interfaces in aquaculture shrimp ponds in a subtropical estuary: Implications for climate warming. Agr. Ecosyst. Environ. 341, 108218. https://doi.org/10.1016/j.agee.2022.108218

Tangen, B.A., Finocchiaro, R.G., Gleason, R.A., Dahl, C.F., 2016. Greenhouse gas fluxes of a shallow lake in south-central North Dakota, USA. Wetlands 36, 779–787.

https://doi.org/10.1007/s13157-016-0782-3

Tong, C., Bastviken, D., Tang, K.W., Yang, P., Yang, H., Zhang, Y.F., Guo, Q.Q., Lai, D.Y.F., 2020. Annual CO_2 and CH_4 fluxes in coastal earthen ponds with *Litopenaeus vannamei* in southeastern China. Aquaculture 545, 737229. https://doi.org/10.1016/j.aquaculture.2021.737229

Tong, C., Morris, J.T., Huang, J.F., Xu, H., Wan, S.A., 2018. Changes in pore-water chemistry and methane emission following the invasion of *Spartina alterniflora* into an oliogohaline marsh. Limnol. Oceanogr. 63, 384–396. https://doi.org/10.1002/lno.10637

Tranvik, L.J., Downing, J.A., Cotner, J.B., Loiselle, S.A., Striegle, R.G., Ballatore, T.J., Dillon, P., Finlay, K., Fortino, K., Knoll, L.B., Kortelainen, P.L., Kutser, T., Larsen, S., Laurion, I., Leech, D.M., McCallister, S.L., McKnight, D.M., Melack, J.M., Overholt, E., Porter, J.A., Prairie, Y., Renwick, W.H., Roland, F., Sherman, B.S., Schindler, D.W., Sobek, S., Tremblay, A., Vanni, M.J., Verschoor, A.M., von Wachenfeldt, E., Weyhenmeyera, G.A., 2009. Lakes and reservoirs as regulators of carbon cycling and climate. Limnol. Oceanogr. 54(6), 2298–2314.

Wang, X.F., He, Y.X., Yuan, X.Z., Chen, H., Peng, C.H., Zhu, Q.A., Yue, J.S., Ren, H.Q., Deng, W., Liu H., 2017. pCO_2 and CO_2 fluxes of the metropolitan river network in relation to the urbanization of Chongqing, China. J. Geophys. Res.- Biogeo., 122(3), 470–486. https://doi.org/10.1002/2016JG003494

Wanninkhof, R., 1992. Relationship between wind-speed and gas-exchange over the ocean. J. Geophys. Res.-Atmos. 97, 7373–7382. https://doi.org/10.1029/92jc00188

Xiao, Q.T., Xu, X.F., Duan, H.T., Qi, T.C., Qin, B.Q., Lee, X.H., Hu, Z.H., Wang, W., Xiao, W., Zhang, M., 2020. Eutrophic Lake Taihu as a significant CO_2 source during 2000–2015. Water Res. 170, 115331. https://doi.org/10.1016/j.watres.2019.115331

Xiong, Y.H., Wang, F., Guo, X,T., Liu, F., Dong, S.L., 2017. Carbon dioxide and methane fluxes across the sediment-water interface in different grass carp *Ctenopharyngodon idella* polyculture models. Aquacult. Environ. Interac. 9, 45–56. https://doi.org/10.3354/aei00214

Xu, C., Su, G.H., Zhao, K.S., Wang, H., Xu, X.Q., Li, Z.Q., Hu, Q., Xu, J., 2023. Assessment of greenhouse gases emissions and intensity from Chinese marine

aquaculture in the past three decades. J. Environ. Manage. 329, 117025. https://doi.org/10.1016/j.jenvman.2022.117025

Xu, H., Paerl, H.W., Zhu, G.W., Qin, B.Q., Hall, N.S., Zhu, M.Y., 2017. Long-term nutrient trends and harmful cyanobacterial bloom potential in hypertrophic Lake Taihu, China. Hydrobiologia 787, 229–242. https://doi.org/10.1007/s10750-016-2967-4

Yang, P., Yang, H., Sardans, J., Tong, C., Zhao, G.H., Peñuelas, J., Ling Li, Zhang, Y.F., Tan, L.S., Chun, K.P., Lai, D.Y.F., 2020a. Large spatial variations in diffusive CH_4 fluxes from a subtropical coastal reservoir affected by sewage discharge in southeast China. Environ. Sci. Technol. 54 (22), 14192–14203. https://doi.org/10.1021/acs.est.0c03431.

Yang, P., Zhang, Y.F., Yang, H., Guo, Q.Q., Lai, D.Y.F., Zhao, G.H., Li, L., Tong, C., 2020b. Ebullition was a major pathway of methane emissions from the aquaculture ponds in southeast China. Water Res. 184, 116176. https://doi.org/10.1016/j.watres.2020.116176.

Yang, P., Zhang, L.H., Lai, D.Y.F., Yang, H., Tan, L.S., Luo, L.J., Tong, C., Hong, Y., Zhu, W.Y., Tang, K.W., 2022a. Landscape change affects soil organic carbon mineralization and greenhouse gas production in coastal wetlands. Global Biogeochem. Cy. 36(12), e2022GB007469. https://doi.org/10.1029/2022GB007469

Yang, P., Tang, K.W., Yang, H., Tong, C., Yang, N., Lai, D.Y.F., Hong, Y., Ruan, M.J., Tan, Y.Y., Zhao, G.H., Li, L., Tang, C., 2022b. Insights into the farming-season carbon budget of coastal earthen aquaculture ponds in southeastern China. Agr. Ecosyst. Environ. 335, 107995. https://doi.org/10.1016/j.agee.2022.107995

Yang, P., Tang, K. W., Tong, C., Lai, D. Y. F., Wu, L. Z., Yang, H., Zhang, L. H., Tang, C., Hong, Y., Zhao, G. H., 2022c. Changes in sediment methanogenic archaea community structure and methane production potential following conversion of coastal marsh to aquaculture ponds. Environ. Pollut. 305, 119276. https://doi.org/10.1016/j.envpol.2022.119276

Yang, P., Lai, D.Y.F., Yang, H., Tong, C., 2019a. Carbon dioxide dynamics from sediment, sediment-water interface and overlying water in the aquaculture shrimp ponds in subtropical estuaries, southeast China. J. Environ. Manag. 236, 224–235. https://doi.org/10.1016/j.jenvman.2019.01.088

Yang, P., Yang, H., Lai, D.Y. F., Jin, B.S., Tong, C., 2019b. Production and uptake of dissolved carbon, nitrogen, and phosphorus in overlying water of aquaculture shrimp ponds in subtropical estuaries, China. Environ. Sci. Pollut. R. 26, 21565–21578. https://doi.org/10.1007/s11356-019-05445-y

Yang, P., Tang, K.W., Yang, H., Tong, C., Zhang, L.H., Lai, D.Y.F., Hong, Y., Tan, L.S., Zhu, W.Y., Tang, C., 2023. Contrasting effects of aeration on methane (CH_4) and nitrous oxide (N_2O) emissions from subtropical aquaculture ponds and implications for global warming mitigation. J. Hydrol. 617, 128876. https://doi.org/10.1016/j.jhydrol.2022.128876

Yan, X.C., Wu, S.J., Xu, J., Xu, X.G., Wang, G.X., 2020. Parallelism of nutrients and CO_2 dynamics: Evidence based on long-term data in Taihu Lake. B. Environ. Contam. Tox. 105, 742–749. https://doi.org/10.1007/s00128-020-03009-2

Yin, S., Bai, J.H., Wang, W., Zhang, G.L., Jia, J., Cui, B.S., Liu, X.H., 2019. Effects of soil moisture on carbon mineralization in floodplain wetlands with different flooding frequencies. J. Hydrol. 574, 1074–1084. https://doi.org/10.1016/j.jhydrol.2019.05.007

Zhang, L., Wang, L., Yin, K.D., Lü, Y., Zhang, D.R., Yang, Y.Q., Huang, X.P., 2013. Pore water nutrient characteristics and the fluxes across the sediment in the Pearl River estuary and adjacent waters, China. Estuar. Coast. Shelf S. 133, 182–192. https://doi.org/10.1016/j.ecss.2013.08.028

Zhang, Y.F., Lyu, M., Yang, P., Lai, D.Y.F., Tong, C., Zhao, G.H., Li, L., Zhang, Y.H., Yang, H., 2021. Spatial variations in CO_2 fluxes in a subtropical coastal reservoir of Southeast China were related to urbanization and land-use types. J. Environ. Sci. 109, 206–218. https://doi.org/10.1016/j.jes.2021.04.003

Zhang, Y.F., Tang, K.W., Yang, P., Yang, H., Tong, C., Song, C.C., Tan, L.S., Zhao, G.H., Zhou, X.D., Sun, D.Y., 2022. Assessing carbon greenhouse gas emissions from aquaculture in China based on aquaculture system types, species, environmental conditions and management practices. Agr. Ecosyst. Environ. 338, 108110. https://doi.org/10.1016/j.agee.2022.108110

Zhang, Y.P., Guo, X.H., Zhu, X.D., 2023. Strong diurnal variability of carbon dioxide flux over algae-shellfish aquaculture ponds revealed by eddy covariance measurements, Agr. Ecosyst. Environ. 348, 108426, https://doi.org/10.1016/j.agee.2023.108426

Table 1 Summary of two-way ANOVAs examining the effects of water depth, month and their interactions on average Chl-*a* and dissolved CO_2 concentrations in the water column of the aquaculture ponds.

	df	Chl-*a* concentration				CO_2 concentration			
		SS	***MS***	***F value***	***P value***	***SS***	***MS***	***F value***	***P value***
Depth	2	930.36	465.18	9.91	0.001	41.51	20.75	12.37	4E-4
Month	9	47359.1	5262.12	112.06	6E-14	969.17	107.69	64.20	7.7E-12
Error	18	845.22	46.96			30.19	1.68		
Total	29	49134.7				1040.87			

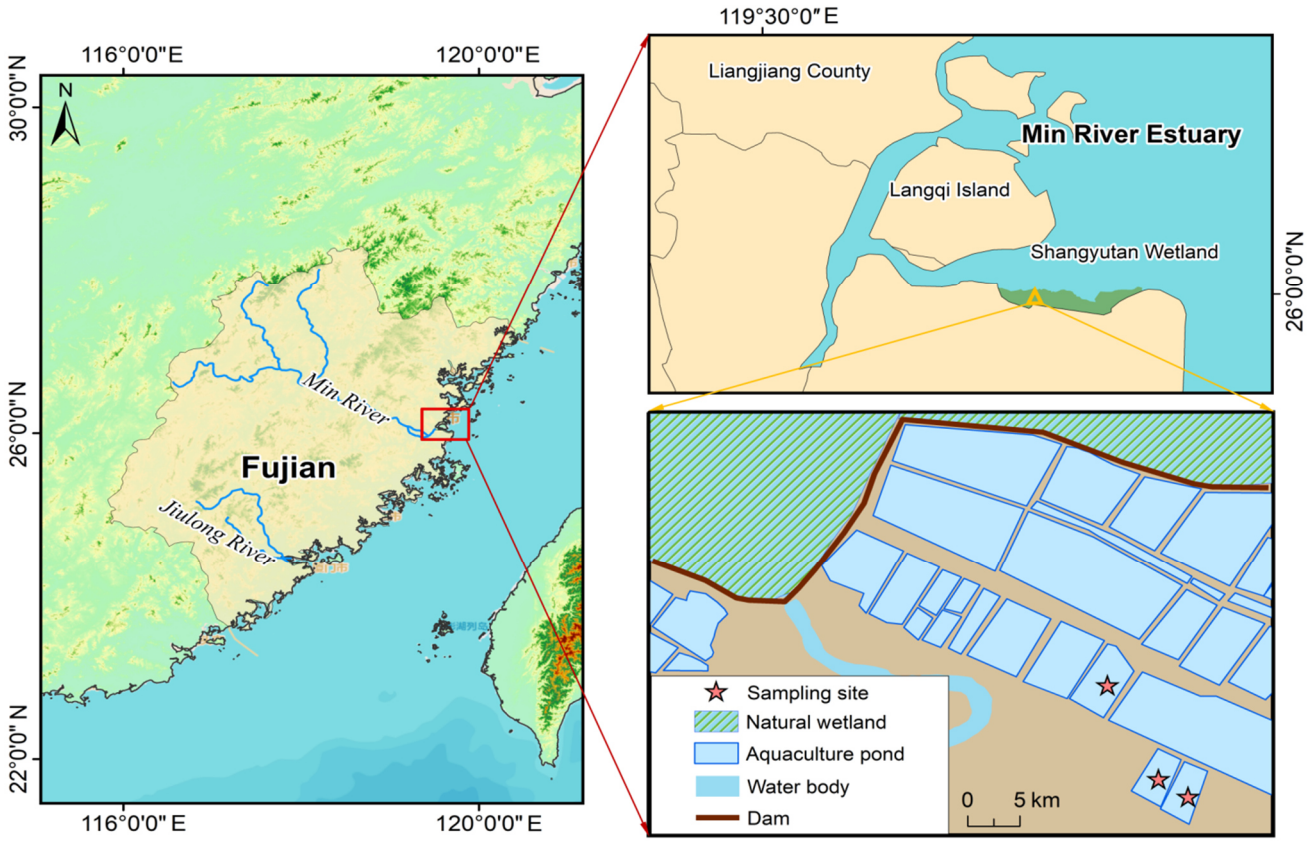

Figure 1. Map of the Shanyutan wetland within the Min River estuary showing the aquaculture ponds used in this study.

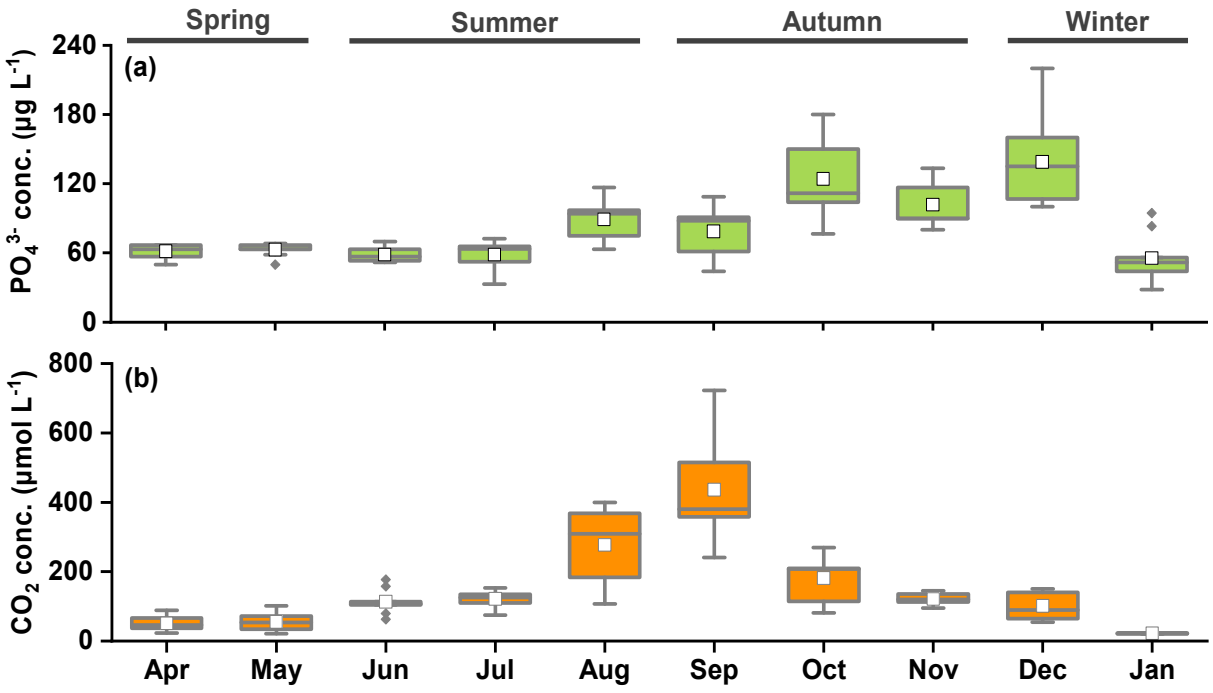

Figure 2. Box plots of monthly values of (a) water-column PO_4^{3-} concentration; and (b) pore-water CO_2 concentrations.

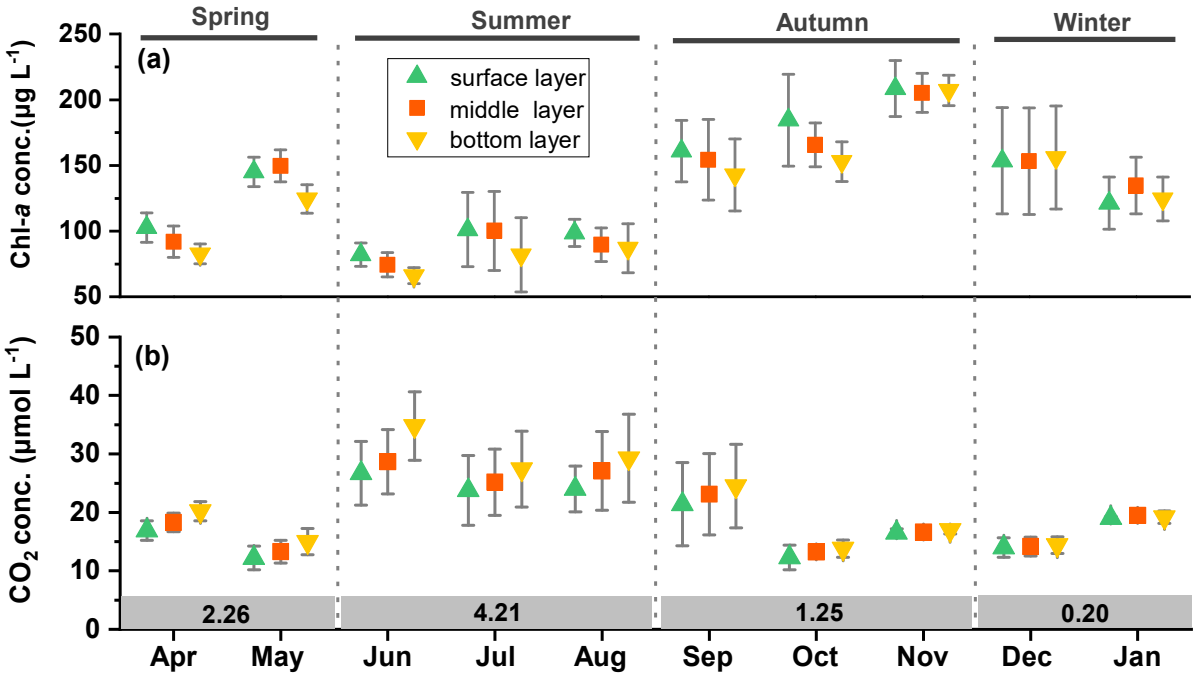

Figure 3. Monthly water column concentrations of (a) chlorophyll-*a* and (b) dissolved CO_2 at different water depths (mean ± SE; n = 9). Numbers within panel b are seasonal average of rate of change in [CO_2] with depth, based on linear regressions. See text and Table S1 for explanation.

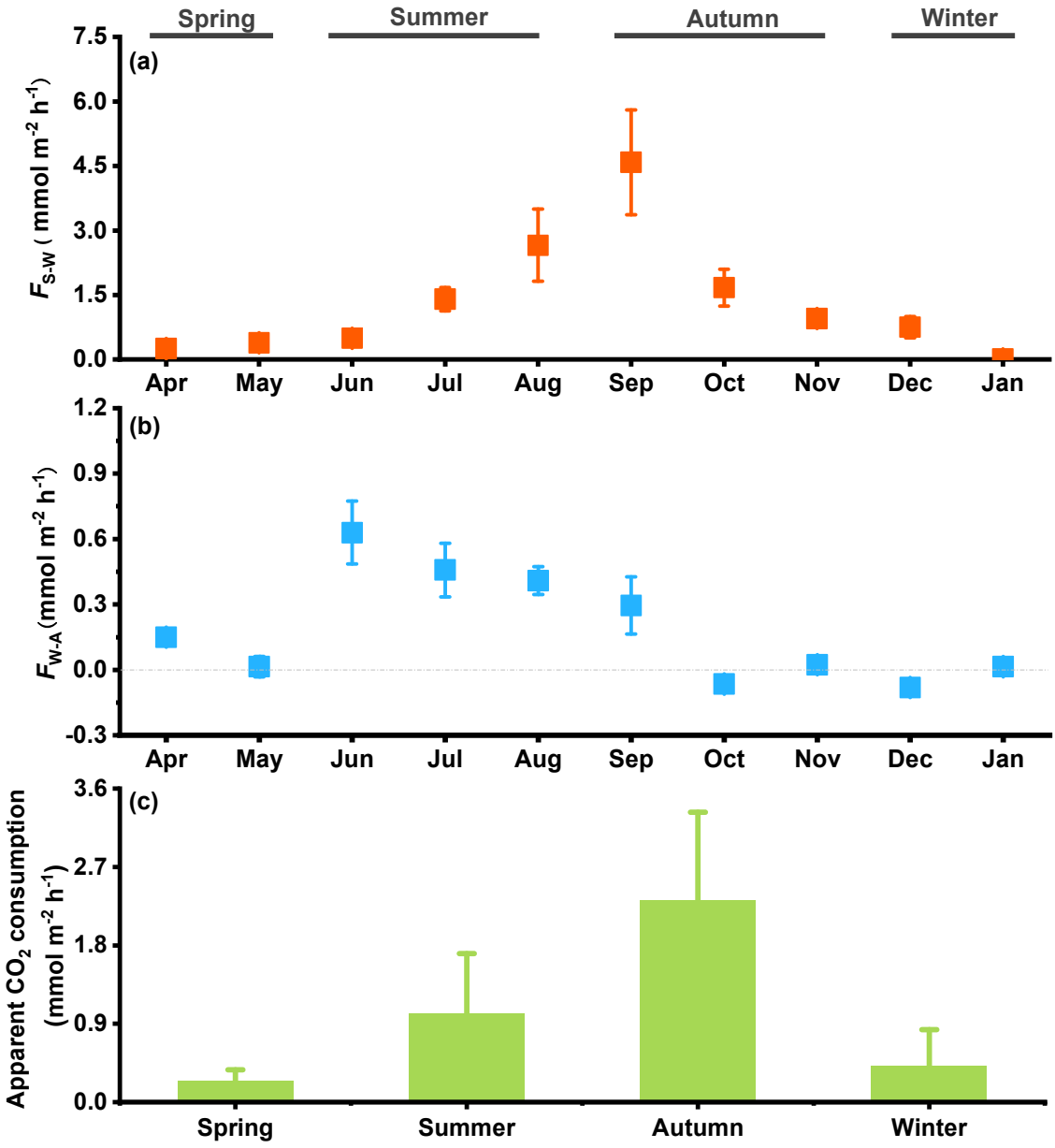

Figure 4. Monthly diffusive CO_2 flux across (a) sediment-water interface and (b) water-air interface (mean ± SE); and (c) seasonal apparent CO_2 consumption within the water column (mean ± SE). See text for explanation.

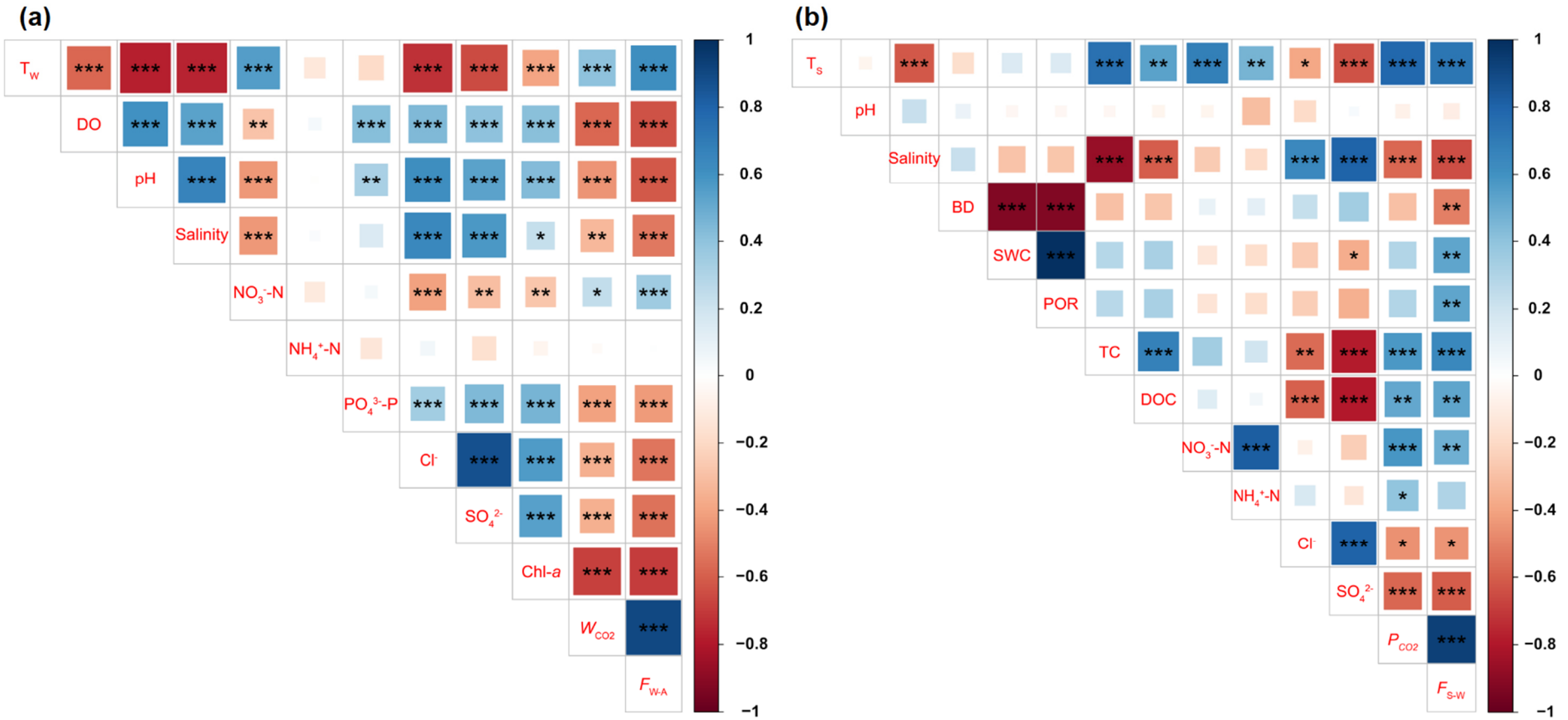

Figure 5. Correlations among environmental and CO_2 variables in (a) water column and (b) sediment. W_{CO2} is water-column CO_2 concentration and $F_{W\text{-}A}$ is CO_2 diffusive flux across the water-air interface. P_{CO2} is porewater CO_2 concentration and $F_{S\text{-}W}$ is CO_2 diffusive flux across the sediment-water interface. Color of the box indicates the direction of correlation (blue = positive; red = negative); size of the box is proportional to the r^2 value. Asterisks indicate levels of significance (*$p < 0.05$; **$p < 0.01$; **$p < 0.001$). See main text for explanation of the abbreviations.

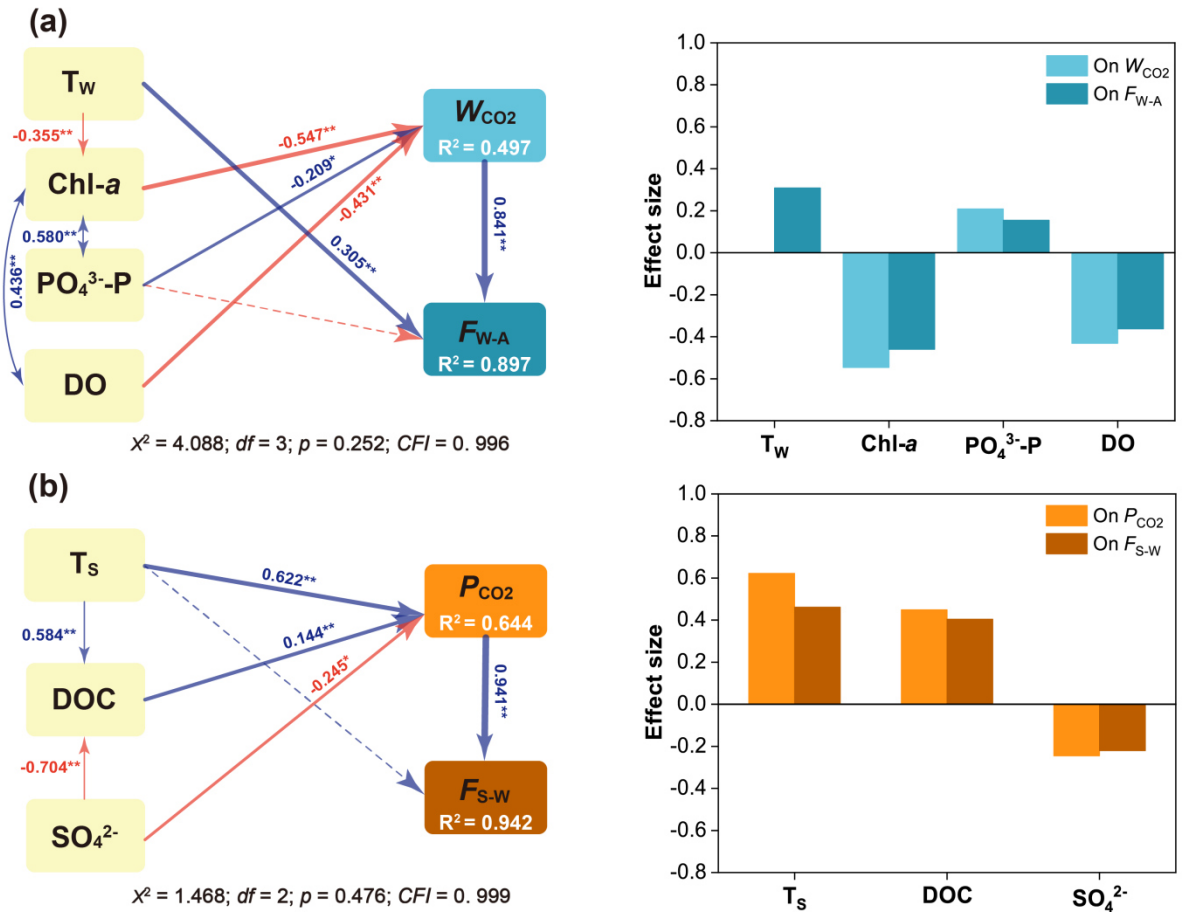

Figure 6. Partial least square structural equation modeling (PLS-SEM) to evaluate the direct and indirect effects of environmental factors on (a) water CO_2 concentration (W_{CO2}) and CO_2 diffusive flux across the water-air interface ($F_{W\text{-}A}$), and (b) sediment porewater dissolved CO_2 concentration (P_{CO2}) and CO_2 diffusive flux across the sediment-water interface ($F_{S\text{-}W}$). Solid blue and red arrows indicate significant positive and negative effects, respectively, and dotted arrow indicates insignificant effect on the dependent variable. Numbers adjacent to arrows are standardized path coefficients, indicating the effect size of the relationship. R^2 represents the variance explained for target variables. * $p < 0.05$; ** $p < 0.01$.

Supporting Information

Seasonal variations in source-sink balance of CO_2 in subtropical earthen aquaculture ponds: Implications for carbon emission management

Lele Tang[a,b], Linhai Zhang[b,c,d], Ping Yang[a,b,c,d*], Chuan Tong[b,c,d], Hong Yang[e], Lishan Tan[f], Yongxin Lin[a,b,c], Derrick Y.F. Lai[f], Kam W. Tang[g*]

[a]*Fujian Provincial Key Laboratory for Subtropical Resources and Environment, Fujian Normal University, Fuzhou 350117, P.R. China*

[b]*School of Geographical Sciences, Fujian Normal University, Fuzhou 350117, P.R. China*

[c]*Key Laboratory of Humid Subtropical Eco-geographical Process of Ministry of Education, Fujian Normal University, Fuzhou 350117, P.R. China*

[d]*Wetland Ecosystem Research Station of Minjiang Estuary, National Forestry and Grassland Administration, Fuzhou 350215, P.R. China*

[e]*Department of Geography and Environmental Science, University of Reading, Reading, UK*

[f]*Department of Geography and Resource Management, The Chinese University of Hong Kong, Hong Kong, China*

[g]*Department of Biosciences, Swansea University, Swansea SA2 8PP, U. K.*

***Correspondence to:**

Ping Yang (yangping528@sina.cn); Kam W. Tang (k.w.tang@swansea.ac.uk)

Supporting Information Summary

No. of pages: 5 No. of Table: 1 No. of Figures: 4

Table S1 Linear regression parameters for Fig. 3b.

Month	$[CO_2]$ *vs* depth linear regression			season avg slope
	slope	intercept	r^2	
April	2.457	16.62	0.999	2.263
May	2.069	11.94	0.996	
June	6.056	25.51	0.952	4.205
July	2.712	23.41	0.994	
August	3.848	23.9	0.974	
September	2.269	21.29	0.984	1.252
October	1.118	12.27	0.952	
November	0.369	16.45	0.972	
December	0.316	13.93	1	0.2
January	0.084	19.17	0.06	

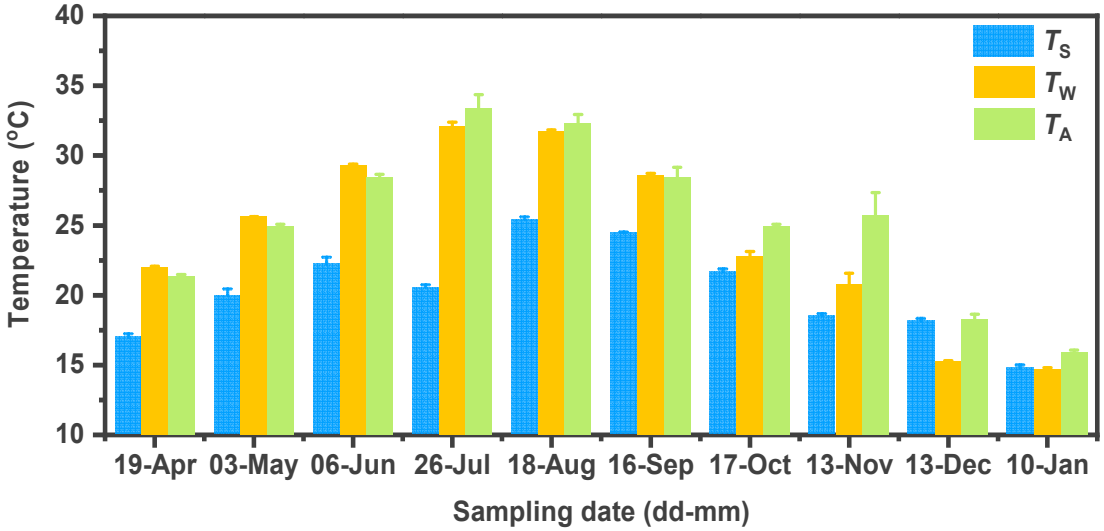

Figure S1 Monthly temperatures in the aquaculture ponds during the farming period (Tian et al., 2023). The bars represent the means + 1 standard error (n = 3 ponds). T_S, T_W and T_A represent sediment temperature, water temperature and air temperature, respectively.

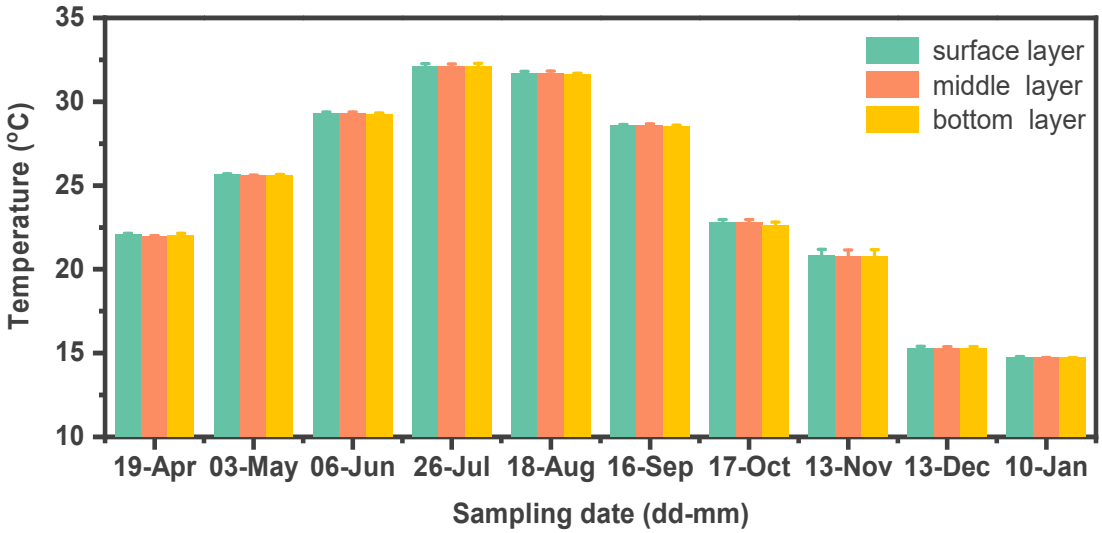

Figure S2. Monthly water temperatures at different depths in the aquaculture ponds during the farming period (mean ± SE; n = 3 ponds).

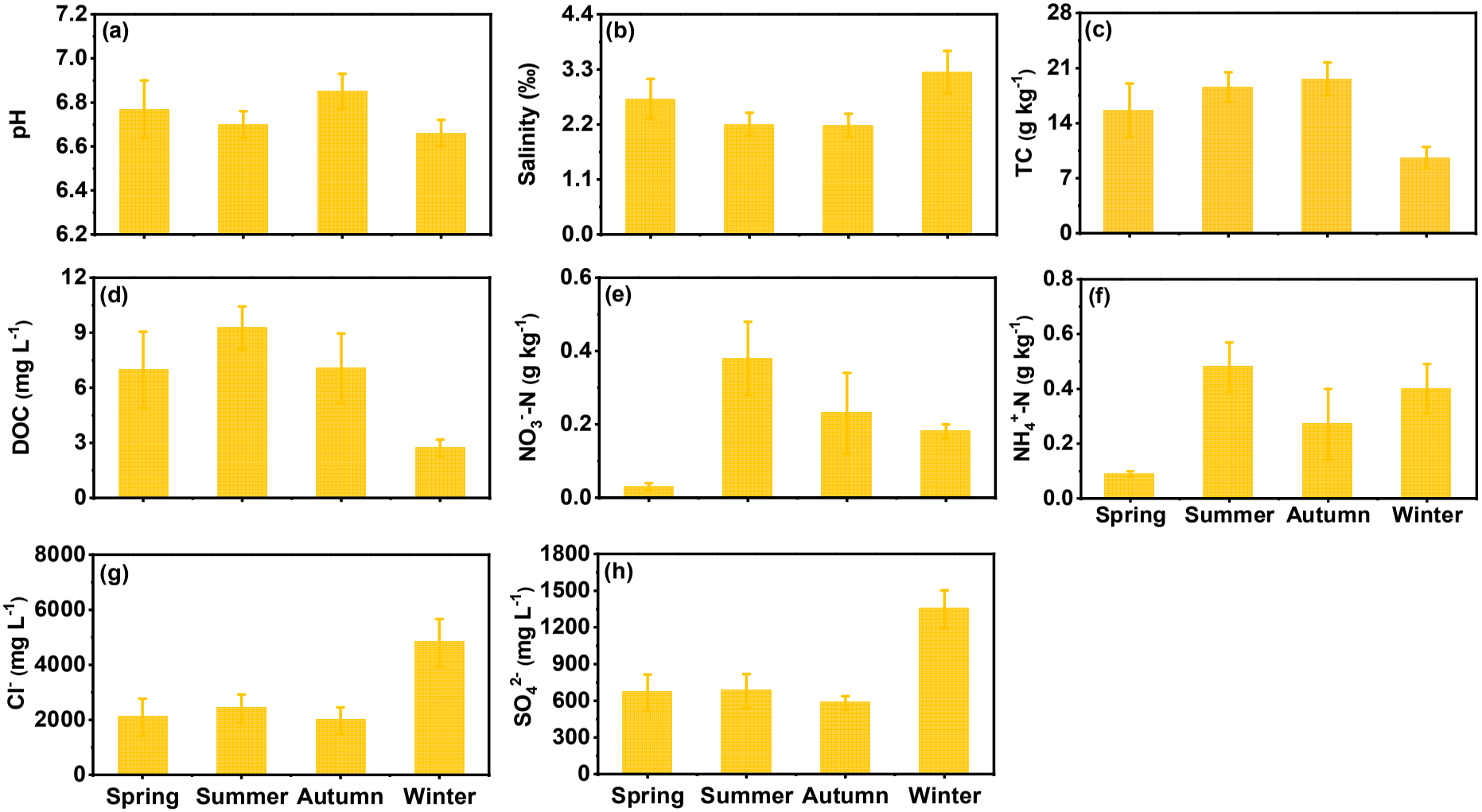

Figure S3 Seasonal values of sediment pH, salinity, total carbon (TC), porewater DOC concentration, NO_3^--N concentration, NH_4^+-N concentration, Cl^- concentration and SO_4^{2-} concentration in the aquaculture ponds during the study period. Data are after Tian et al. (2023) and Yang et al. (2022) for reference and review only.

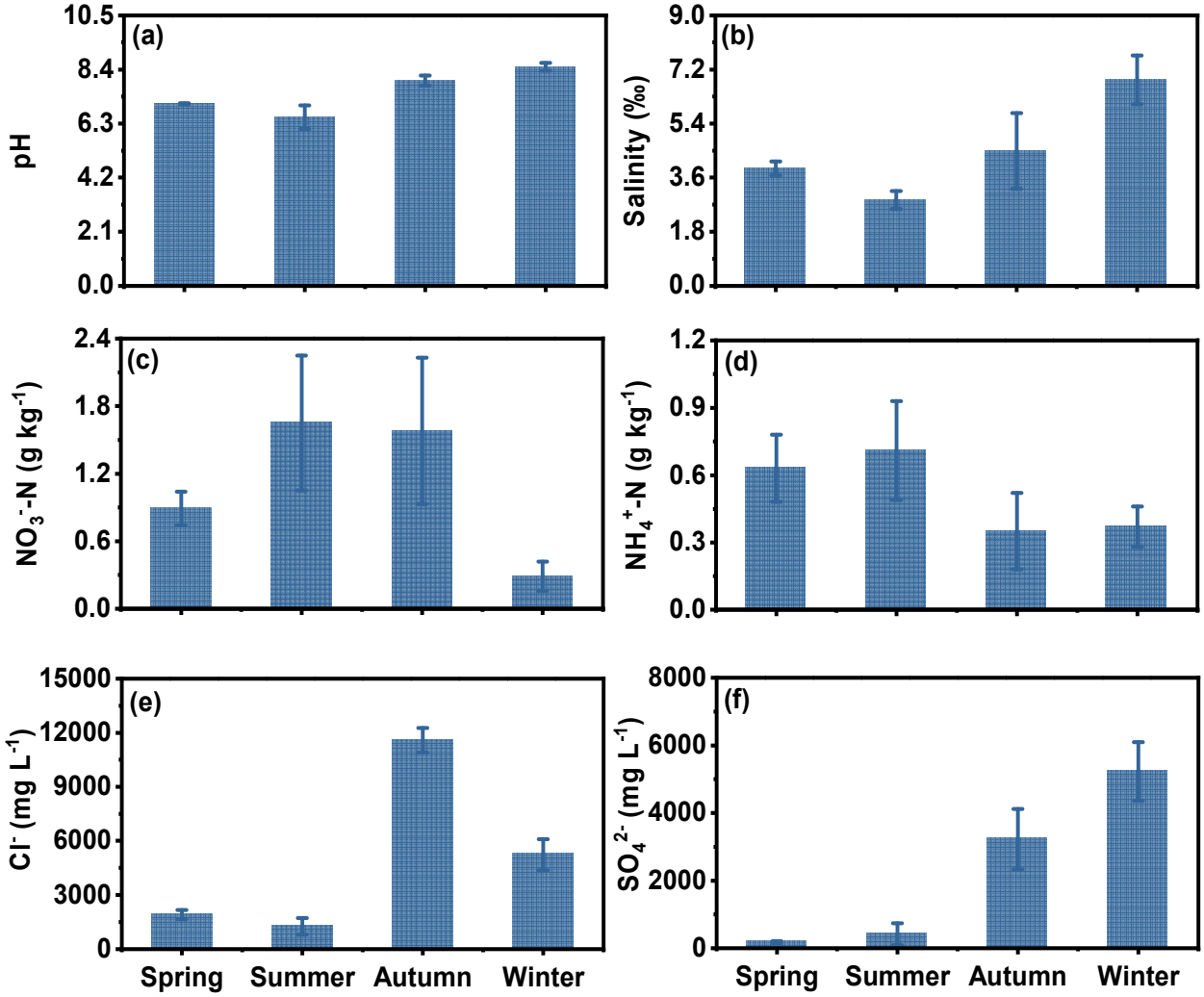

Figure S4 Seasonal values of pH, salinity, NO_3^--N, NH_4^+-N, Cl^- and SO_4^{2-} concentration in water column of the aquaculture ponds during the study period. Data are after Tian et al. (2023) and Yang et al. (2022) for reference and review only.

References

Tian, Y.L, Yang, P., Yang, H., Wang, H.M., Zhang, L.H., Tong, C., Lai, D.Y.F., Lin, Y.X., Tan, L.S., Hong, Y., Tang, C., Tang, K.W., 2023. Diffusive nitrous oxide (N_2O) fluxes across the sediment-water-atmosphere interfaces in aquaculture shrimp ponds in a subtropical estuary: Implications for climate warming. Agr. Ecosyst. Environ. 341, 108218. https://doi.org/10.1016/j.agee.2022.108218

Yang, P., Tang, K. W., Tong, C., Lai, D. Y. F., Wu, L. Z., Yang, H., Zhang, L. H., Tang, C., Hong, Y., Zhao, G. H., 2022c. Changes in sediment methanogenic archaea community structure and methane production potential following conversion of coastal marsh to aquaculture ponds. Environ. Pollut. 305, 119276. https://doi.org/10.1016/j.envpol.2022.119276

Author Contribution Statement

Conceptualization: Ping Yang, Kam W. Tang, Chuan Tong, Derrick Y. F. Lai

Methodology: Lele Tang, Ping Yang, Linhai Zhang, Yongxin Li, Wenjing Liu, Lihua Wang

Formal analysis: Lele Tang, Lishan Tan, Derrick Y. F. Lai, Yongxin Li

Validation: Ping Yang

Investigation: Lele Tang, Linhai Zhang, Ping Yang, Wenjing Liu, Lihua Wang,

Data Curation: Ping Yang, Kam W. Tang, Chuan Tong

Writing-Original Draft: Lele Tang, Ping Yang, Kam W. Tang

Writing - Review & Editing: Ping Yang, Kam W. Tang

Project Administration: Ping Yang, Chuan Tong

Funding acquisition: Ping Yang, Chuan Tong